Estimates of Precession and Polar Motion Errors from Planetary Encounter Station Location Solutions

G. E. Pease
Navigation Systems Section

Jet Propulsion Laboratory Deep Space Station (DSS) location solutions based on two JPL planetary ephemerides, DE 84 and DE 96, at eight planetary encounters have been used to obtain weighted least squares estimates of precession and polar motion errors. The solution for precession error in right ascension yields a value of $0.3 \times 10^{-5} \pm 0.8 \times 10^{-6}$ *deg/year. This maps to a right ascension error of* $1.3 \times 10^{-5} \pm 0.4 \times 10^{-5}$ *deg at the first Voyager 1979 Jupiter encounter if the current JPL DSS location set is used. Solutions for precession and polar motion using station locations based on DE 84 agree well with the solution using station locations referenced to DE 96. The precession solution removes the apparent drift in station longitude and spin axis distance estimates, while the encounter polar motion solutions consistently decrease the scatter in station spin axis distance estimates.*

I. Introduction

In the course of JPL DSS location determination, many sources of systematic error have been identified and modeled in order to improve the accuracy of the estimates. The largest errors were traced to the planetary ephemerides, polar motion and timing, tropospheric refraction, and charged particle effects. Dramatic improvements have been made in these areas through the use of more refined radar ephemerides, BIH polar motion and timing corrections, interstation and seasonal tropospheric corrections, and Faraday rotation, differenced range versus integrated doppler (DRVID), and S-X dual frequency calibrations. The addition of recent planetary encounter data (Mariner 10 at Venus and Mercury, Vikings 1 and 2 at Mars) has greatly increased the quantity and time span of planetary encounter tracking data from which station locations may be determined.

Current location sets (Ref. 1) utilize tracking data from Mariners 4, 5, 6, 9, and 10 planetary encounters of Mars, Venus, and Mercury to obtain combined estimates referenced to JPL ephemerides, DE 84 and DE 96. In addition, Campbell and Rinker (Ref. 2) have estimated station location corrections relative to Location Set (LS) 44 from Viking 1 and 2 Mars encounter tracking data. Planetary encounter station location solutions are thus now available over an 11-year span, from Mariner 4 in 1965 to Viking in 1976.

The station longitude solutions (Figs. 1 and 3) reveal an apparent secular drift of about -0.3×10^{-5} deg/year over the 11-year span. Lieske (Ref. 3) has predicted an apparent station longitude drift of this size due to the known error in Newcomb's constant of general precession.

Fliegel and Wimberly (Ref. 4) have shown that BIH polar motion errors could be greater than 1 meter, if systematic errors are considered in addition to observational scatter. Such an error at a planetary encounter would affect the spin axis distance and longitude estimates of all DSN tracking stations.

For this report, DSS longitude and spin axis distance solutions (Figs. 1-4) from eight planetary encounters were used to estimate the precession error and individual encounter polar motion errors. The DE 84 and DE 96 solutions agree very closely. The solution for precession yields a correction of $0.31 \times 10^{-5} \pm 0.8 \times 10^{-6}$ deg/year in right ascension, which is essentially Lieske's predicted correction. The consequent predicted right ascension error at the first Voyager 1979 Jupiter encounter is $1.3 \times 10^{-5} \pm 0.4 \times 10^{-5}$ deg. The values obtained from DE 84 and DE 96 locations differ by only 0.1×10^{-6} deg/year. It appears likely, therefore, that the principal source of error is in the transformation from the equinox and equator of 1950.0 to the equinox and equator of date at the planetary encounter times for the computed doppler and range observables. This includes errors from rigid-body approximations in the nutation. These may be significant in the large-amplitude term having an 18.6-year period. As seen in Fig. 5, the nutation in celestial longitude is almost linear from Mariner 4 encounter where it is −15.″2 on July 15, 1965, to Mariner 10 Venus encounter, Feb. 5, 1974, where it is +18.″8. For this 8½-year span, a 0.1% error in the long-period nutation terms would contribute 0.″034 error, or about 0.1×10^{-5} deg/year. The contribution, if any, of "equinoctial drift" is unknown.

II. Data Equations and Partial Derivatives

Polar motion corrections X and Y, in radians, are approximated in Ref. 5 as follows:

$$\lambda = \lambda_0 + \frac{Z_0}{r_{s_0}}(X \sin \lambda_0 + Y \cos \lambda_0), \tag{1}$$

$$r_s = r_{s_0} - Z_0 (X \cos \lambda_0 - Y \sin \lambda_0), \tag{2}$$

where

λ_0 = uncorrected Greenwich east longitude of tracking station, in radians

r_{s_0} = uncorrected distance of tracking station from Earth's spin axis

Z_0 = distance of tracking station from Earth's equator

The correction X is measured south along the 1903.0 meridian of zero longitude; Y is measured south along the 90°W meridian of 1903.0. For the purposes of this paper, these corrections are in the form of corrections to the BIH Circular D smoothed values (see Ref. 4).

The partial derivatives of interest are, therefore,

$$\partial r_s / \partial X = -Z_0 \cos \lambda_0 , \tag{3}$$

$$\partial r_s / \partial Y = Z_0 \sin \lambda_0 , \tag{4}$$

$$\partial \lambda / \partial X = \frac{Z_0}{r_{s_0}} \sin \lambda_0 , \tag{5}$$

$$\partial \lambda / \partial Y = \frac{Z_0}{r_{s_0}} \cos \lambda_0 , \tag{6}$$

It is seen that the above partial derivatives are functions only of 1903.0 station cylindrical coordinates Z_0, λ_0, and r_{s_0}.

Precession corrections (Ref. 6) are

$$P_\alpha = m + n \sin \alpha \tan \delta, \tag{7}$$

$$P_\delta = n \cos \alpha, \tag{8}$$

where

m = the precession in right ascension

n = the precession in declination

α = the right ascension of the spacecraft at planetary encounter

δ = the spacecraft declination at planetary encounter

The appropriate station location corrections (see Ref. 7) are, to first order,

$$\lambda = \lambda_0 + \dot{\alpha}_\gamma (t - t_0)(1 + \tan \epsilon \sin \alpha \tan \delta), \tag{9}$$

$$r_s = r_{s_0} + \dot{\delta}_\gamma (t - t_0) r_{s_0} \cos \alpha \tan \delta, \tag{10}$$

where (see Fig. 6)

ϵ = the obliquity of the ecliptic

t = planetary encounter time

t_0 = reference time at which a station location set is free of precession error

$\dot{\alpha}_\gamma$ = observed error in m, from station longitude estimates

$\dot{\delta}_\gamma$ = observed error in n, from station spin axis distance estimates

The partial derivatives are then,

$$\frac{\partial \lambda}{\partial \dot{\alpha}_\gamma} = (t - t_0)(1 + \tan \epsilon \sin \alpha \tan \delta), \tag{11}$$

$$\frac{\partial r_s}{\partial \dot{\delta}_\gamma} = (t - t_0) r_{s_0} \cos \alpha \tan \delta, \tag{12}$$

$$\frac{\partial \lambda}{\partial t_0} = -\dot{\alpha}_\gamma (1 + \tan \epsilon \sin \alpha \tan \delta), \tag{13}$$

$$\frac{\partial r_s}{\partial t_0} = -\dot{\delta}_\gamma r_{s_0} \cos \alpha \tan \delta. \tag{14}$$

III. Least Squares Formulation

The data equation is

$$z = Ax + \eta = \begin{bmatrix} r_s(i) \\ \lambda(i) \end{bmatrix}, \quad i = \text{DSS index} \tag{15}$$

$$x = [X, Y, \dot{\alpha}_\gamma, \dot{\delta}_\gamma, t_0]^T, \tag{16}$$

$$A = \left[\frac{\partial z_i}{\partial x}\right], \tag{17}$$

where x is the 5×1 vector of estimated parameters and A is the $2i \times 5$ mapping matrix, with i equal to the number of tracking stations for which r_s and λ estimates are input. The normalized data equation,

$$\bar{z} = \bar{A}x + \bar{\eta}, \tag{18}$$

is used where

$$[\bar{A}, \bar{z}] = w^{-1/2} [A, z], \tag{19}$$

and

w = the covariance weighting matrix of observables.

Introducing a priori information

$$\tilde{R}\,\tilde{x} = \tilde{z}, \tag{20}$$

where R is the a priori square root information matrix,

$$\begin{bmatrix} \tilde{R} & \tilde{z} \\ \bar{Z} & \bar{z} \end{bmatrix} \text{ orthogonal } = [R\,\hat{z}], \tag{21}$$

$$[R\,\hat{z}]^{-1} = [R^{-1}, \hat{x}] = [P^{1/2}, \hat{x}], \tag{22}$$

where $\hat{x}$ is the estimate of the polar motion and precession parameters and P is the covariance on the estimate.

Bierman and Nead's Estimation Subroutine Package (ESP) was used for the upper triangular matrix computations (Refs. 8, 9). The program incorporating these routines was written by F. H. Brady for the specific problem of using encounter station location estimates to obtain estimates of precession and polar motion parameters and to plot the residuals.

IV. Computational Procedure

The computations were organized to process station location λ and r_s residuals (Figs. 1-4), adding one encounter set at a time. The upper rows correspond to the polar motion parameters, X and Y. By zeroing and initializing the upper two rows with $\tilde{R}(X,Y)$ before each encounter, an independent estimate of X and Y is obtained at each encounter while the precession parameters $\dot{\alpha}_\gamma$, δ_γ, and t_0 are sequentially estimated. The final values of $\dot{\alpha}_\gamma$, $\dot{\delta}_\gamma$, and t_0 are then used to obtain smoothed estimates of X and Y for each encounter. New λ and r_s residuals from the smoothed estimates are then plotted.

V. Data Weighting

Diagonal weighting matrices were used to obtain the results of this paper. These weights are the "consider" variances of the location estimates associated with LS 44 (Ref. 1) and the Viking solutions (Ref. 2). They are tabulated in Table 1. Special weights were adopted for DSS 41 at Mariner 5 Venus encounter and DSS 42 at Mariner 10 Mercury I encounter as a result of weak λ and r_s solutions for these passes. These weights more realistically represent the actual scatter in the station location solutions compared with the "consider" variances.

VI. A Priori Uncertainties

A priori uncertainties for the estimated parameters were input, based on information in Refs. 3 and 4. For the results

of this paper the following a priori standard deviations were assumed:

$$\sigma_X, \sigma_Y = 0.2 \text{ rad} = 1.27 \text{ meters}$$

$$\sigma_{\dot{\alpha}_\gamma} = 2. \times 10^{-13} \text{ deg/sec} = 0.63 \times 10^{-5} \text{ deg/year}$$

$$\sigma_{\dot{\delta}_\gamma} = 1. \times 10^{-13} \text{ deg/sec} = 0.32 \times 10^{-5} \text{ deg/year}$$

$$\sigma_{t_0} = 0.1 \times 10^{9} \text{ sec} = 1157.4 \text{ days}$$

VII. Polar Motion Solutions

Three solutions for polar motion were performed. Two of these used station location estimates based on DE 84 (Figs. 1 and 2). The first DE 84 solution was for polar motion only and did not include precession parameters. The other DE 84 solution estimated polar motion and precession parameters and used the final precession solution to obtain smoothed polar motion estimates. The third solution obtained smoothed polar motion estimates in the same fashion, but used station location estimates based on DE 96 (Figs. 3 and 4). These solutions are summarized in Table 2.

It is seen that the solutions are in good agreement, with the exception of the Mariner 4 and Mariner 6 solutions for X, in which the polar-motion-only solution yields substantially smaller values than the smoothed solution. The good agreement between DE 84 and DE 96 solutions for X and Y is especially interesting, the implication being that if ephemeris errors are contributing heavily to the polar motion solutions, then both DE 84 and DE 96 have very similar errors.

The uncertainties on these X and Y estimates range from 0.4 to 1.1 meters, running about 0.7 meter for the most part. No seasonal trends are evident in the solutions, other than a noticeable peak in the Y solutions in the months of July and August.

Figures 7 and 8 are the λ and r_s residual plots after the solution for polar motion only. Comparing Figures 1 and 7, no improvement is evident in the longitude residuals, with the exception of the Mariner 6 and Viking 1 residuals. They display slightly less scatter, but other encounters show slightly increased scatter, if anything. The r_s residuals, however, are significantly improved by the solution for polar motion only. This is quite evident, comparing Figures 2 and 8. The square root of the weighted sum of squares (SRWSOS) of all λ and r_s residuals dropped from 8.37 before the fit to 7.73 after the fit for polar motion only.

VIII. Precession Solutions

The precession solutions are summarized in Table 3. For the runs which included polar motion in the solutions, essentially the value predicted by Reference 4 was obtained. The agreement between DE 84 and DE 96 $\dot{\alpha}_\gamma$ solutions is excellent. The most significant difference is in the t_0 solutions, which differ by 6 months, or about 0.6σ. This is equivalent to a small system rotation of inner planet right ascensions between DE 84 and DE 96 of about 0.16×10^{-5} deg, or 0".006. This once again represents remarkable agreement between DE 84 and DE 96.

The solution for just precession error yields a slightly smaller correction in $\dot{\alpha}_\gamma$ than the solutions which include polar motion (see Table 3). In the precession-only solution, the square root of the weighted sum of squares of λ and r_s residuals was reduced from 8.37 before the fit to 7.35 after the fit.

The sequential solutions for precession parameters $\dot{\alpha}_\gamma$, $\dot{\delta}_\gamma$ and t_0 are respectively plotted in Figs. 9, 10, and 11. The excellent agreement between DE 84 and DE 96 solutions is once again apparent. The precession-only solution displays a less systematic nature in $\dot{\delta}_\gamma$ and t_0 (Figs. 10 and 11). The plotted points for all three sets of solutions represent the results of adding encounter station location solutions cumulatively, one encounter at a time.

Referring to Fig. 5, it is tempting to speculate that some of the systematic nature of Figs. 9, 10, and 11 may be due to an error in the 18.6-year period nutation term.

The results obtained from precession and smoothed polar motion estimates are plotted in Figs. 12-15. The square root of the weighted sum of squares of the DE 84 λ and r_s residuals dropped from 8.37 before the fit to 5.92 after the smoothed fit. The SRWSOS of the DE 96 residuals dropped from 8.33 before the fit to 5.84 after the smoothed fit.

IX. Conclusions

DSS location solutions at eight planetary encounters have been used to obtain weighted least squares estimates of precession and polar motion errors. The indicated precession correction in right ascension is 0.31×10^{-5} deg/year $\pm 0.8 \times 10^{-6}$ deg/year, essentially the value predicted by Lieske in Ref. 3. This corresponds to a predicted right ascension error of $1.3 \times 10^{-5} \pm 0.4 \times 10^{-5}$ deg at the first Voyager 1979 Jupiter encounter. The solutions for precession and polar motion errors

using station locations based on DE 84 agree well with the solution using station locations referenced to DE 96.

The degree to which ephemeris error contributes to these solutions is unknown. However, the consistency between DE 84 and DE 96 solutions suggests that contributing ephemeris errors are largely common to both DE 84 and DE 96. The degree to which nutation error contributes to the precession solution is also unknown, but it is likely that nutation error is a principal cause of the systematic nature of the sequential solutions for precession error, possibly contributing as much as 0.1×10^{-5} deg/year in $\dot{\alpha}_\gamma$.

Acknowledgments

I wish to thank F. H. Brady, who wrote the computer program used to obtain these results, and G. J. Bierman and H. M. Koble, who gave invaluable assistance in organizing the filter algorithms appropriate to this problem.

References

1. Koble, H. M., Pease, G. E., and Yip, K. W., "LS 44 – An Improved Deep Space Network Station Location Set for Viking Navigation," in *The Deep Space Network Progress Report 42-35*, Jet Propulsion Laboratory, Pasadena, Calif., Oct. 15, 1976.

2. Campbell, J. K., and Rinker, G. C., "An Evaluation of Deep Space Network Station Locations from the Viking Encounters," Engineering Memorandum 314-107, Jet Propulsion Laboratory, Pasadena, Calif., Jan. 11, 1977 (an internal document).

3. Lieske, J., "Effect of Precession and Nutation Errors on Radar Observations," in *Space Program Summary 37-54, Vol. III*, Jet Propulsion Laboratory, Pasadena, Calif., Nov. 30, 1968.

4. Fliegel, H. F., and Wimberly, R. N., *Time and Polar Motion*, Technical Report 32-1587, Jet Propulsion Laboratory, Pasadena, Calif., Mar. 1, 1974.

5. Moyer, T. D., *Mathematical Formulation of the Double-Precision Orbit Determination Program (DPODP)*, Technical Report 32-1527, Jet Propulsion Laboratory, Pasadena, Calif., May 15, 1971.

6. *The American Ephemeris and Nautical Almanac for the Year 1974*, U. S. Government Printing Office, Washington, D. C., 1972, p. 9.

7. Hamilton, T. W., and Melbourne, W. G., "Information Content of a Single Pass of Doppler Data from a Distant Spacecraft," in *Space Program Summary 37-39, Vol. III*, Jet Propulsion Laboratory, Pasadena, Calif., May 31, 1966.

8. Bierman, G. J., and Nead, M. W., "An Estimation Subroutine Package: Part 1 – Parameter Estimation," Engineering Memorandum 314-4, Jet Propulsion Laboratory, Pasadena, Calif., Sept. 20, 1976 (an internal document).

9. Bierman, G. J., *Factorization Methods for Discrete Sequential Estimation*, Academic Press, 1977.

Table 1. Diagonal elements of $w(\sigma^2_{r_s}, \sigma^2_{\lambda})$

DSS	Encounter							
	M4	M5	M6	M9	M10 Venus	M10 Merc I	Vik 1	Vik 2
$\sigma^2_{r_s}$ (meters)^2								
11	.4476						.7225	1.0201
12		18.6710	5.8709	1.2499	.8263	4.4100		
14		1.9321	6.7133	16.717	.5155	.2510	2.4964	.7396
41		16.[a]	4.2271	.7604				
42	.4160				1.337	16.[a]		.6400
43					.3318	.1190	.7744	.7396
51	.4942		6.9116					
61							1.0000	.4096
62		1.7716	3.4559	.8742	1.2860	1.0962		
63					.3919	.1340	.5776	
$\sigma^2_{\lambda}(10^{-5}$ deg)^2								
11	2.1993						1.9044	1.0816
12		27.6781	1.6053	4.5156	7.7562	2.5824		
14		74.4251	1.8117	8.6318	7.5900	1.1342	2.8900	1.4884
41		64.[a]	1.3948	3.1791				
42	1.9155				8.5031	64.[a]		1.0000
43					7.5735	1.1172	1.6384	1.5129
51	1.6384		3.0241					
61							2.1316	1.0816
62		19.5100	1.8279	4.5924	9.6100	1.7082		
63					7.6452	1.1236	1.8496	

[a]An a priori weight

Table 2. Planetary encounter polar motion solutions

Encounter	Date	X (JPL − BIH) meters			Y (JPL − BIH) meters		
		DE 84 PM only	DE 84 Smoothed	DE 96 Smoothed	DE 84 PM only	DE 84 Smoothed	DE 96 Smoothed
Mariner 4	07/15/65	.46	1.83	1.23	.57	.85	.99
Mariner 5	10/19/67	.36	.74	.82	.39	.40	.52
Mariner 6	07/31/69	−.71	.13	.42	.99	1.02	.73
Mariner 9	11/14/71	−1.39	−1.64	−1.93	−.40	−.55	−.54
Mar 10 Ven	02/05/74	−.29	−.34	−.56	−.10	−.08	−.44
Mar 10 Mer	03/29/74	.09	.11	.38	−.30	−.33	−.24
Viking 1	06/19/76	.41	.38	.30	−.46	−.08	.01
Viking 2	08/07/76	−.90	−1.44	−1.11	.25	.75	.66

Table 3. Planetary encounter secular right ascension and declination drifts, Mariner 4 through Viking 2

Solution	$\dot{\alpha}_\gamma$ (10^{-5} deg/yr)	$\dot{\delta}_\gamma$ (10^{-5} deg/yr)	t_0
DE 84, polar motion not in solution	−.268 ±.072	.297 ±.218	10/14/74 ±281 days
DE 84, polar motion in solution	−.321 ±.079	.286 ±.237	06/08/74 ±319 days
DE 96, polar motion in solution	−.310 ±.079	.377 ±.237	12/05/74 ±319 days

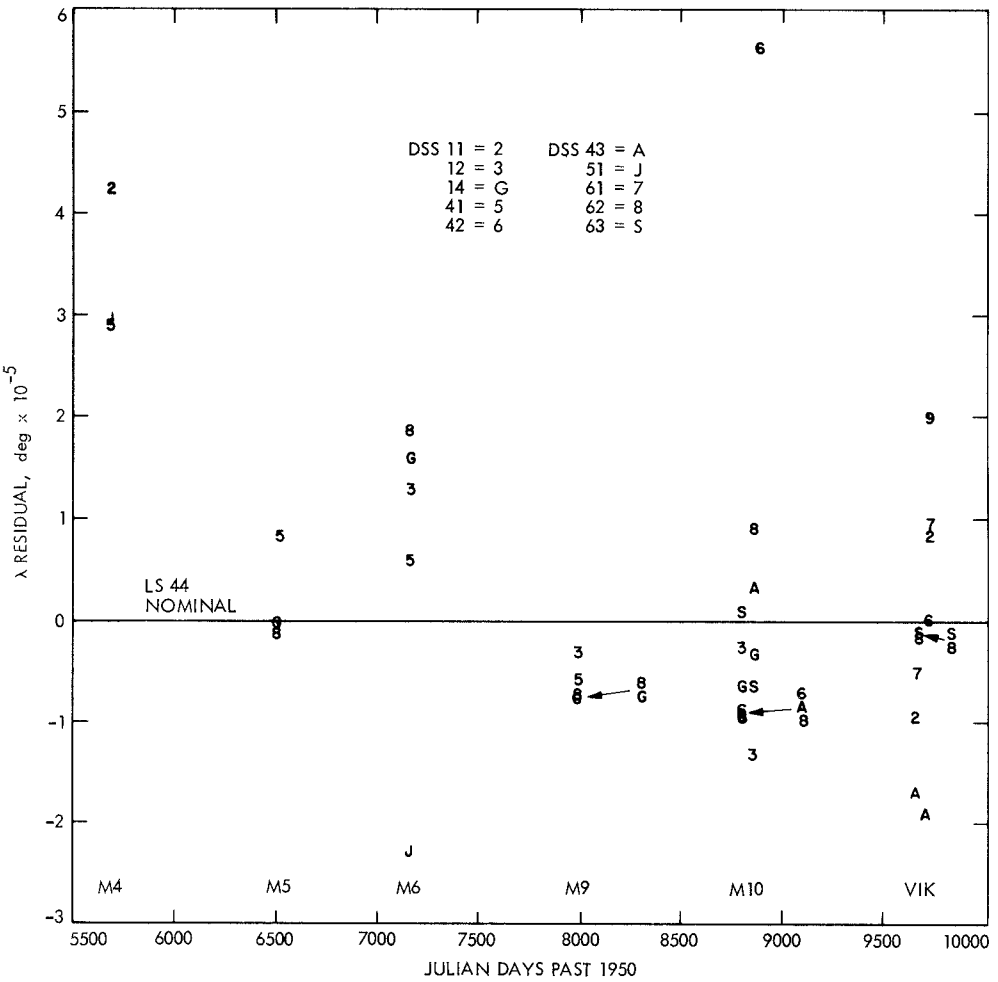

Fig. 1. DE 84 input λ residuals

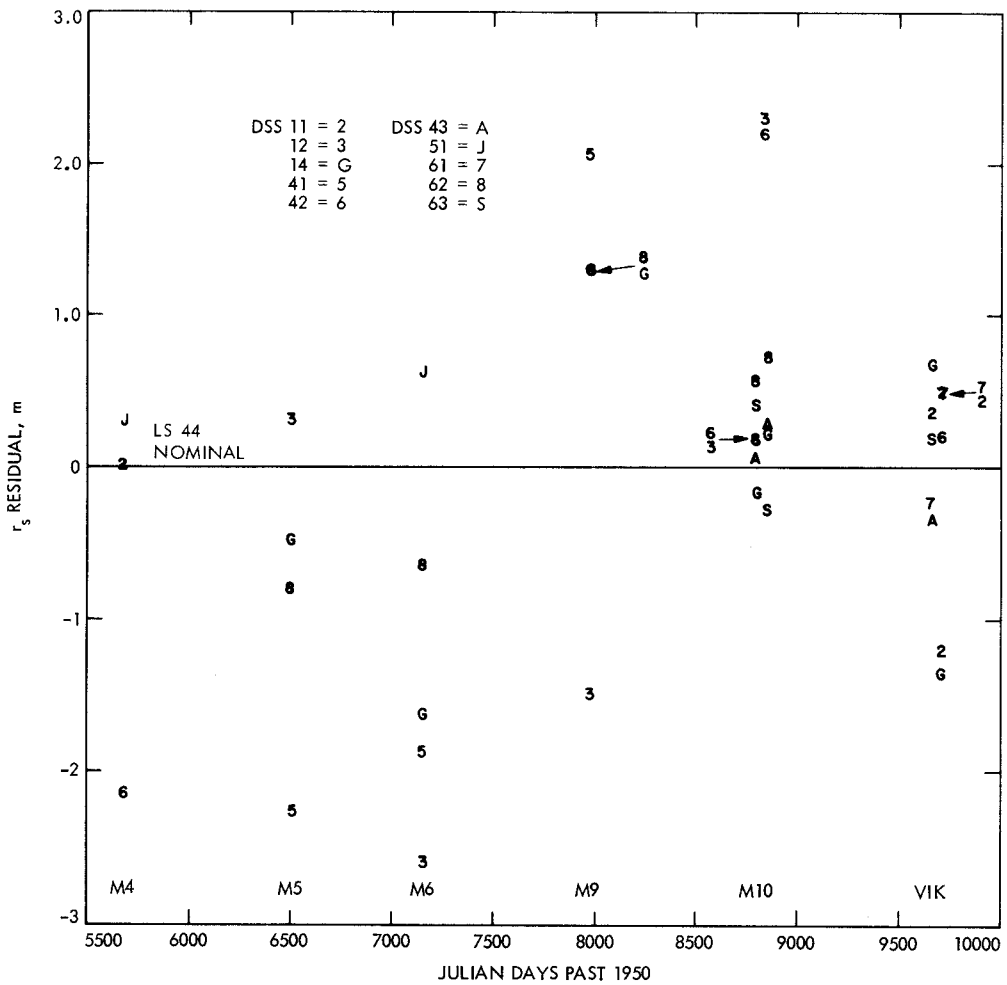

Fig. 2. DE 84 input r_s residuals

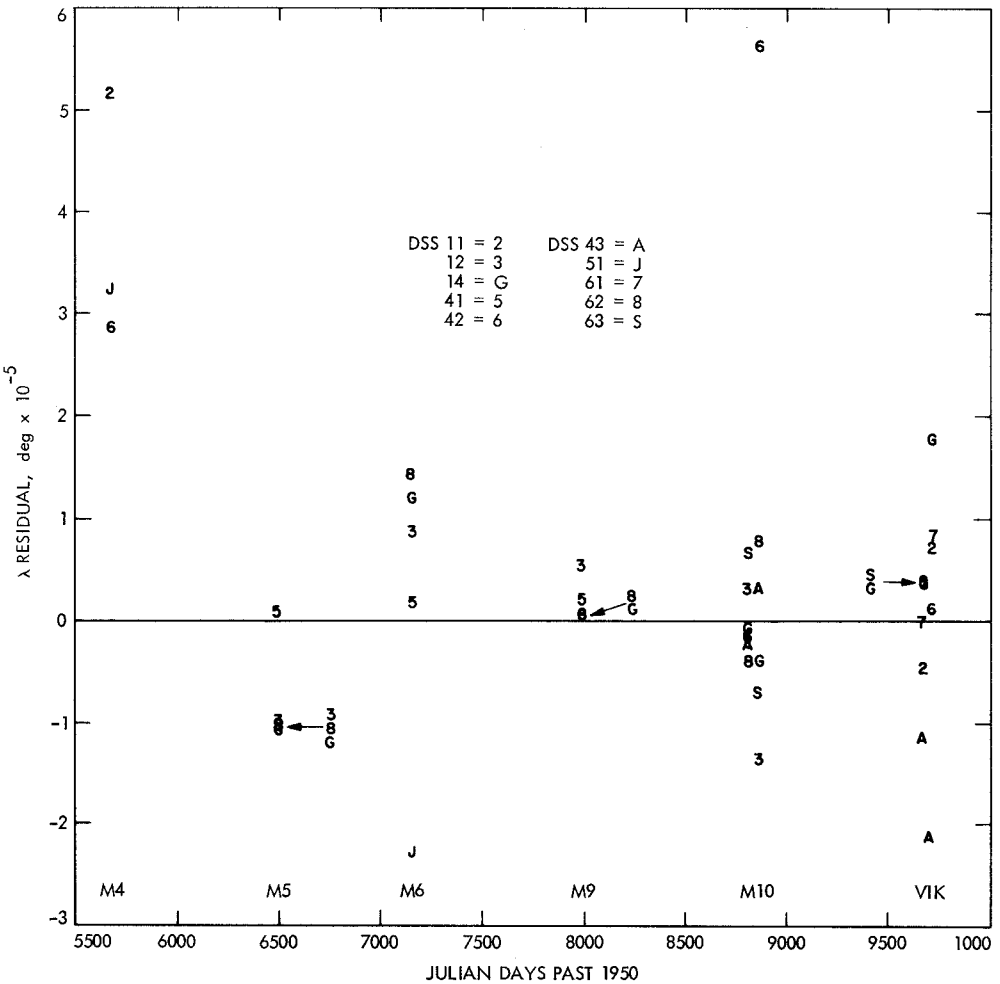

Fig. 3. DE 96 input λ residuals

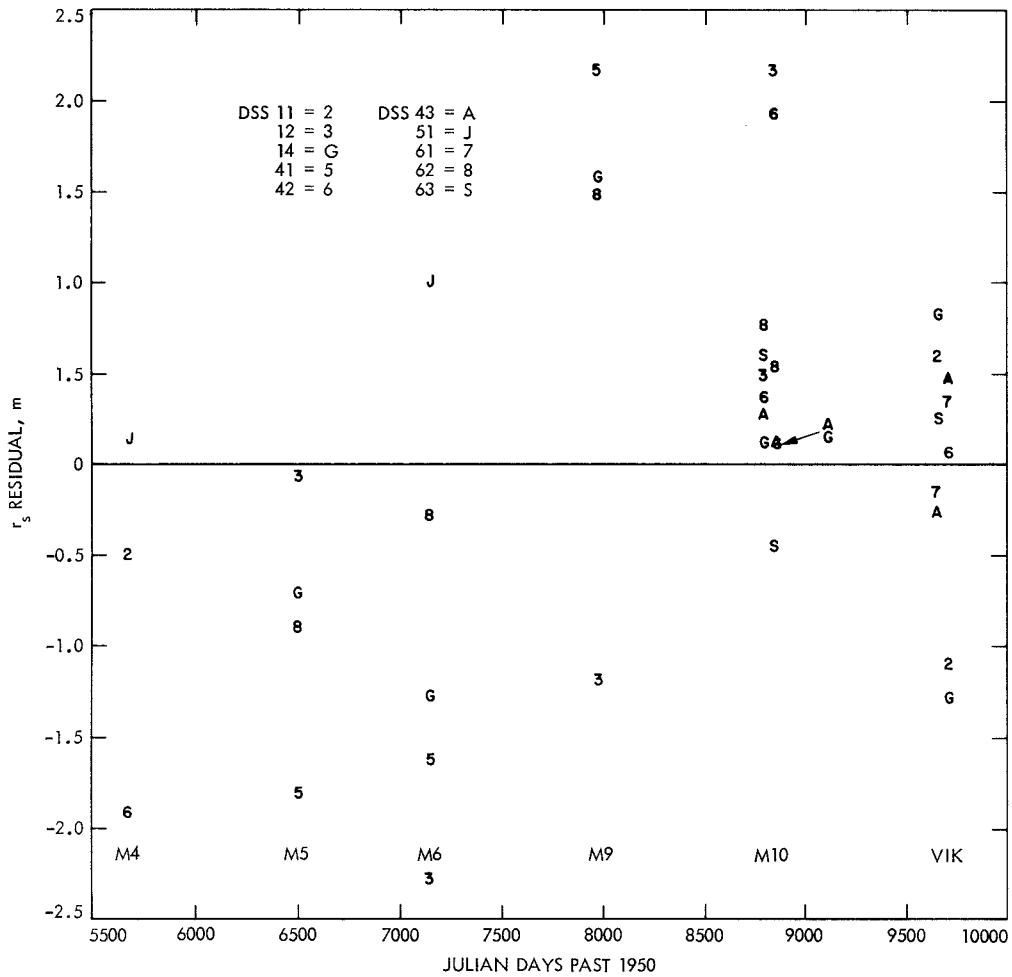

Fig. 4. DE 96 input r_s residuals

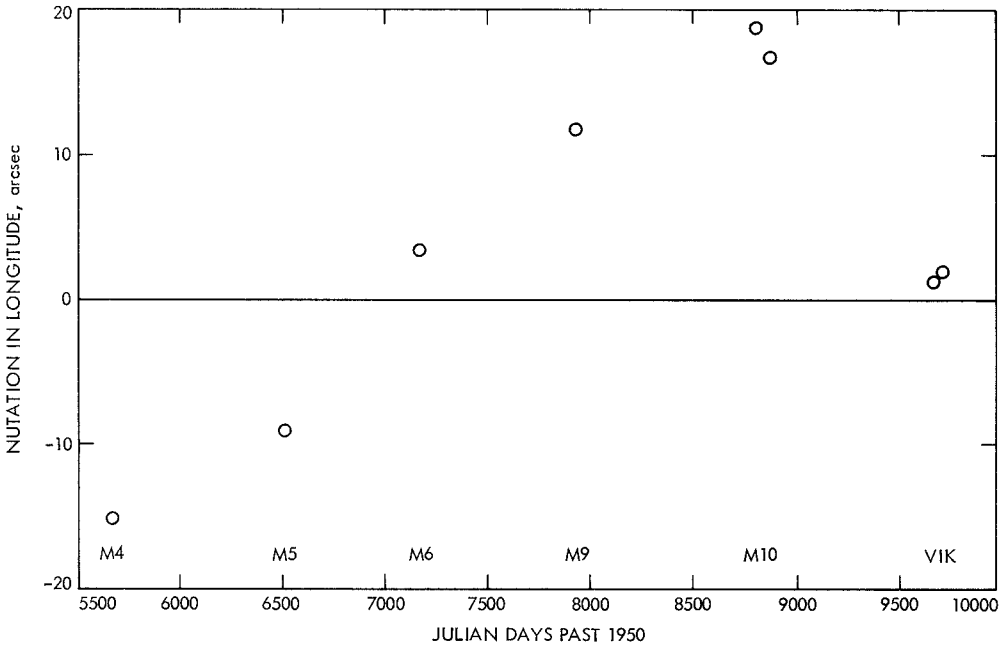

Fig. 5. Nutation in celestial longitude at planetary encounters

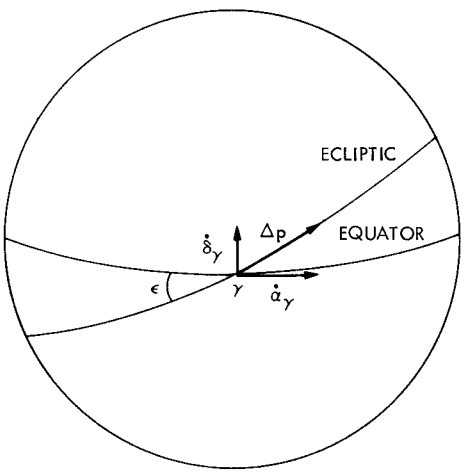

Fig. 6. Celestial sphere showing precession errors, $\dot{\alpha}_\gamma$, $\dot{\delta}_\gamma$

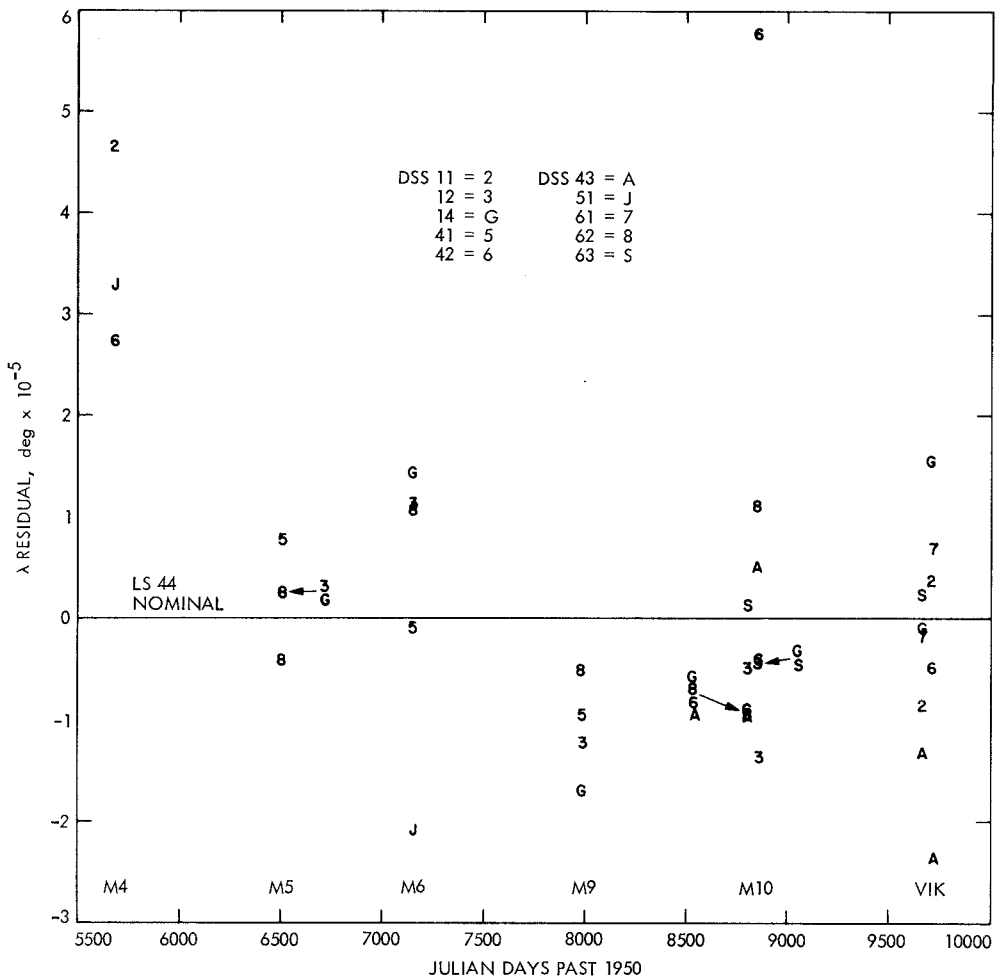

Fig. 7. DE 84 λ residuals after estimating polar motion only

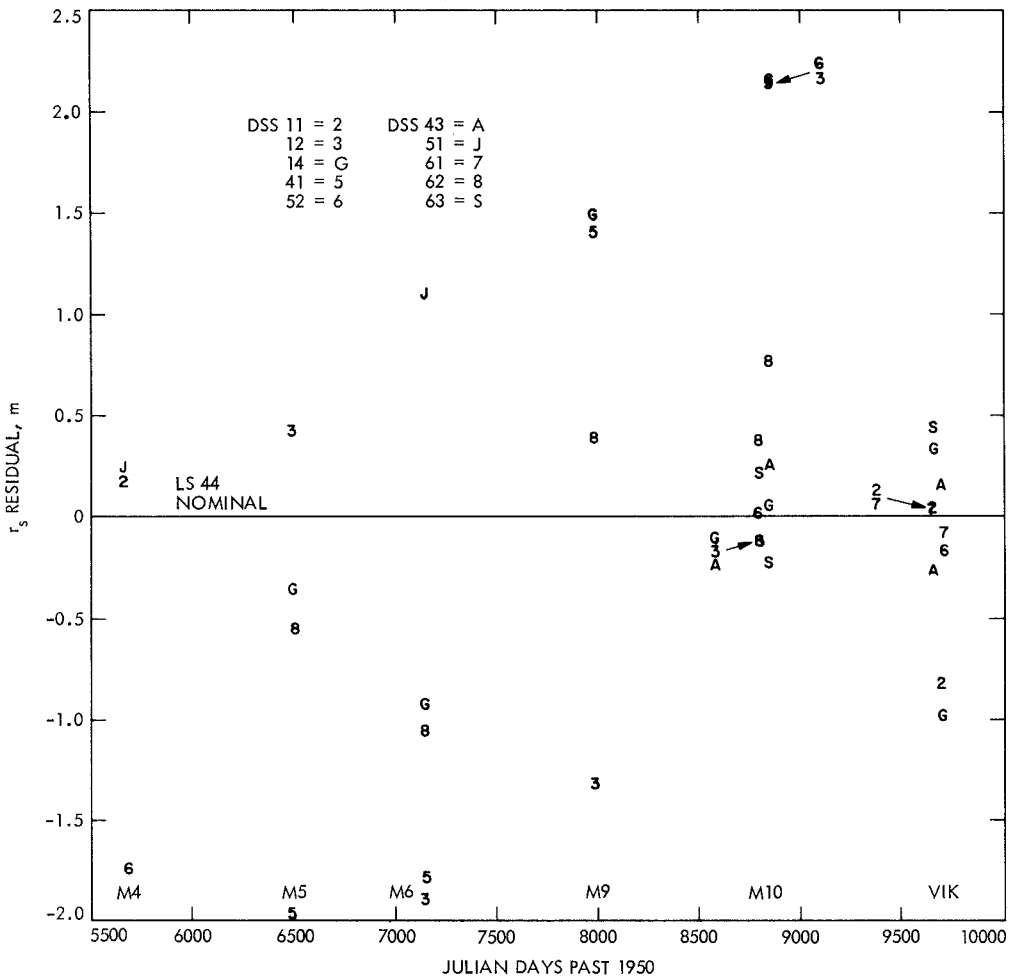

Fig. 8. DE 84 r_s residuals after estimating polar motion only

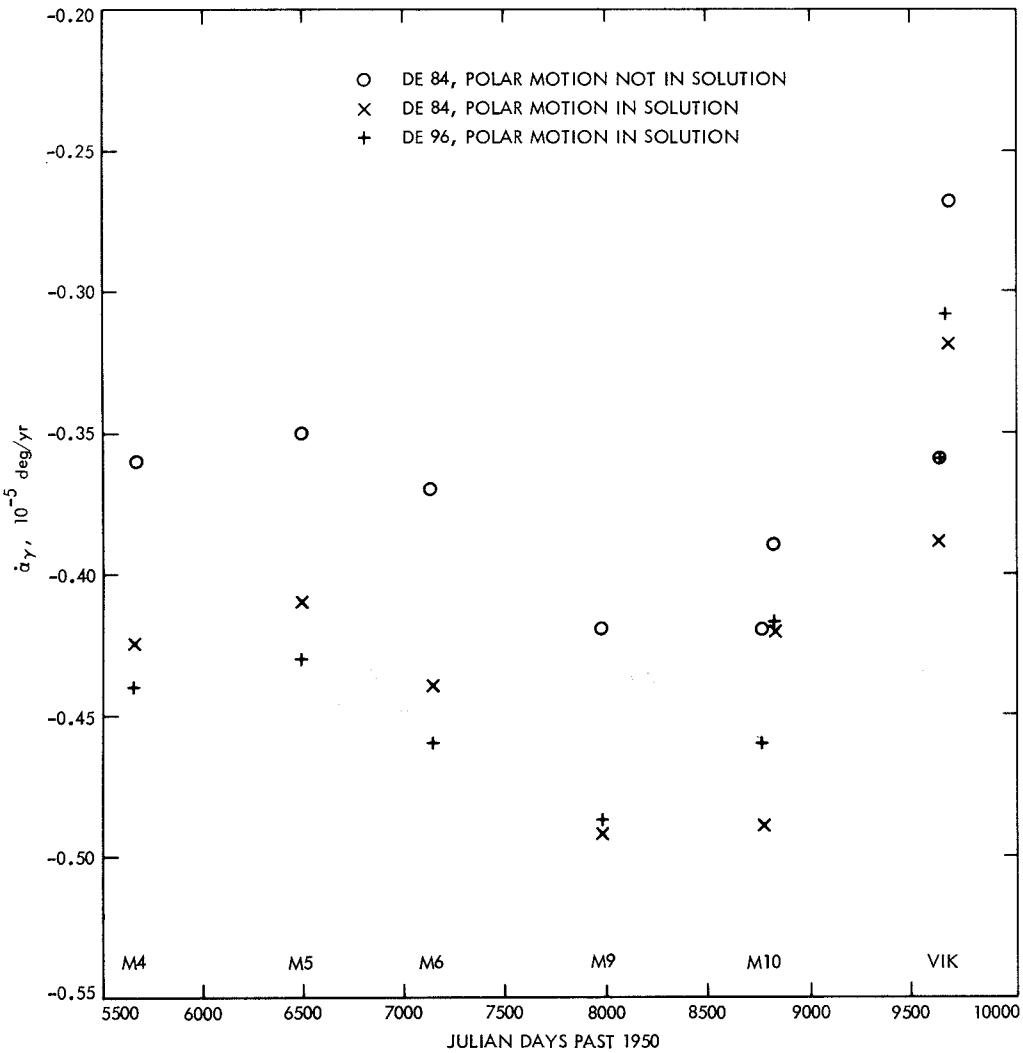

Fig. 9. Sequential solutions for right ascension drift, $\dot{\alpha}_\gamma$

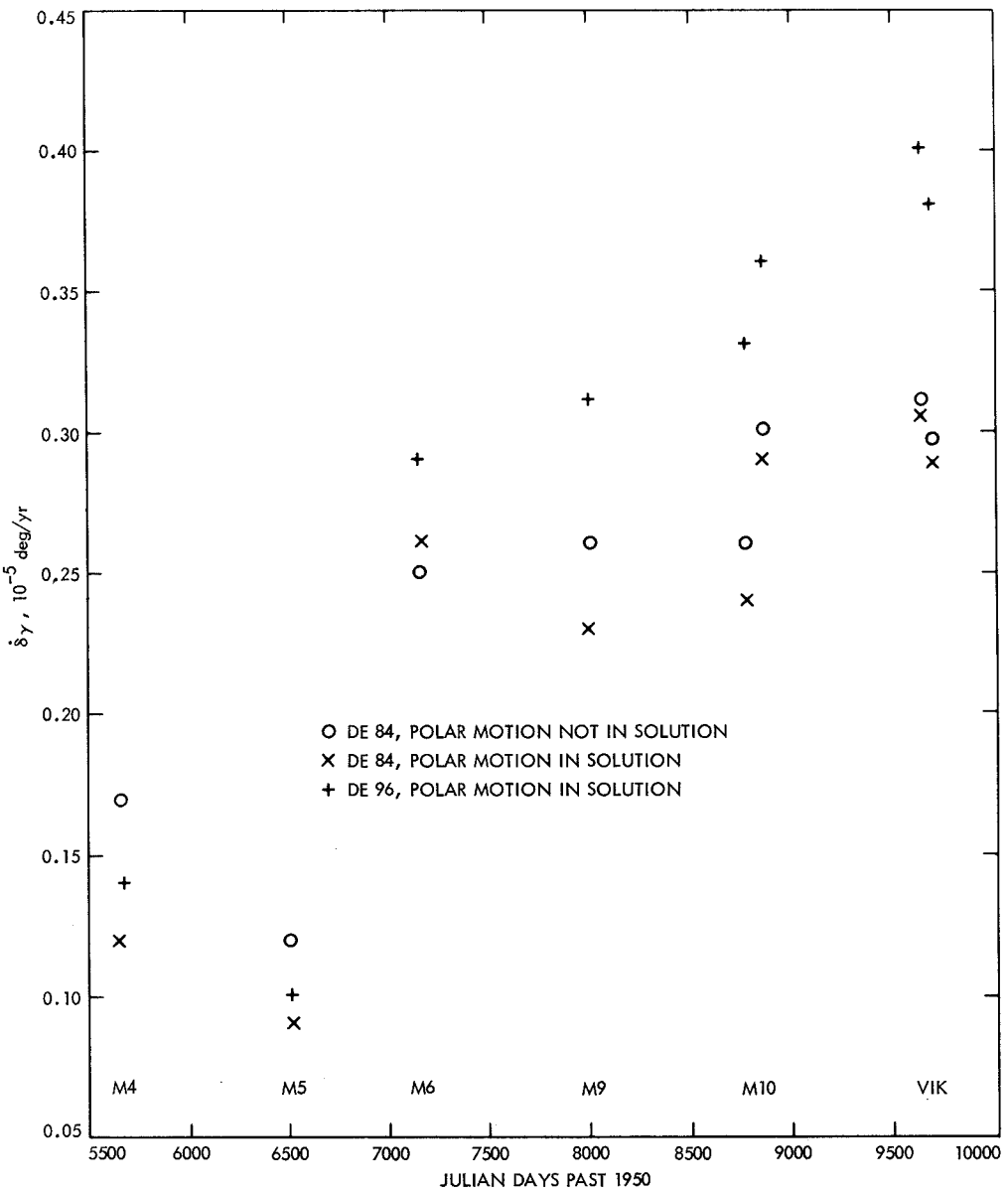

Fig. 10. Sequential solutions for declination drift, $\dot{\delta}_\gamma$

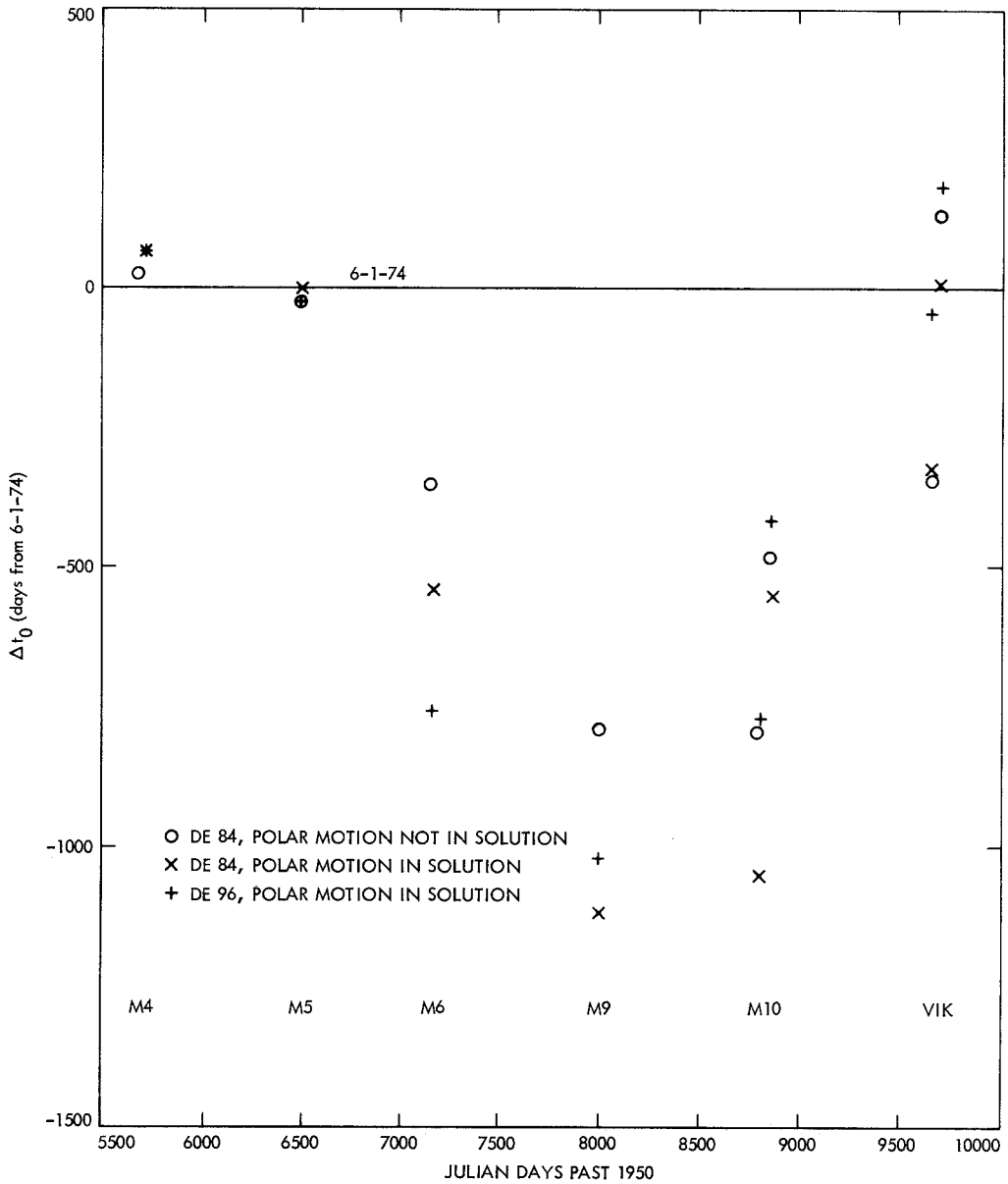

Fig. 11. Sequential solutions for equinox drift epoch, t_0

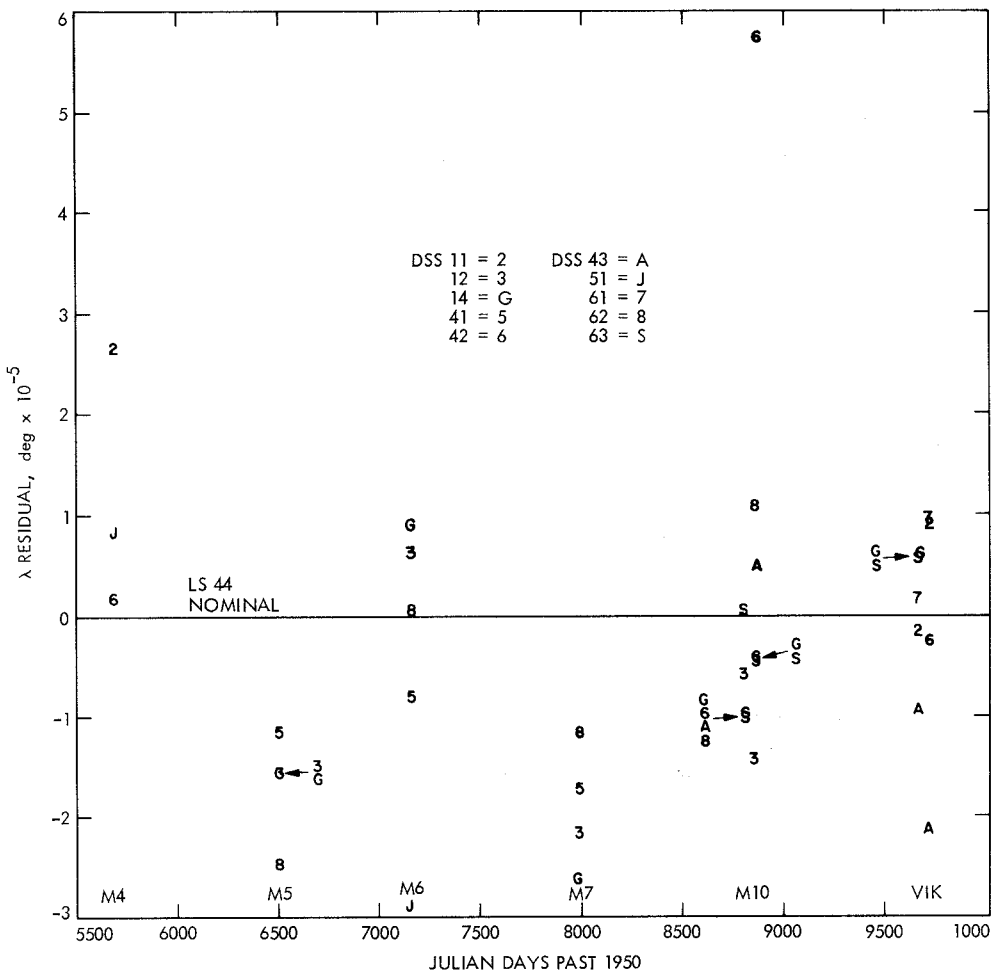

Fig. 12. DE 84 λ residuals after estimating precession and smoothed polar motion

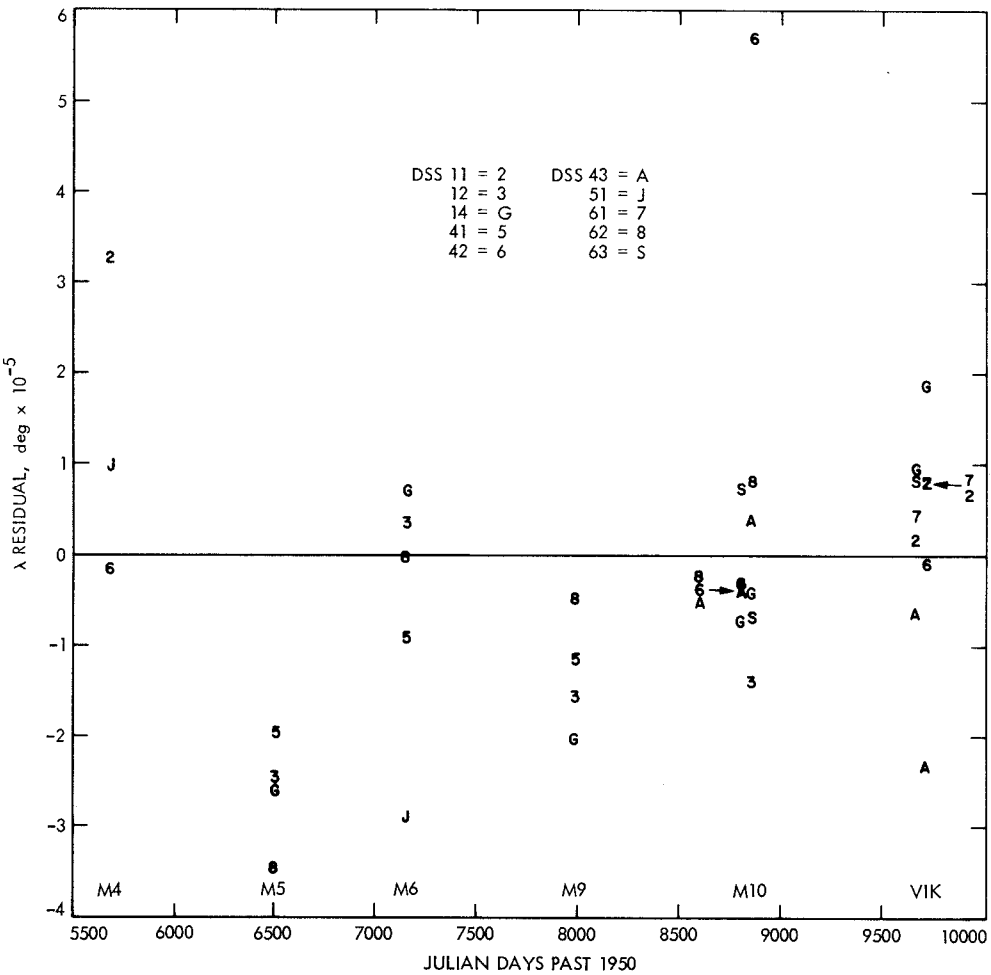

Fig. 13. DE 96 λ residuals after estimating precession and smoothed polar motion

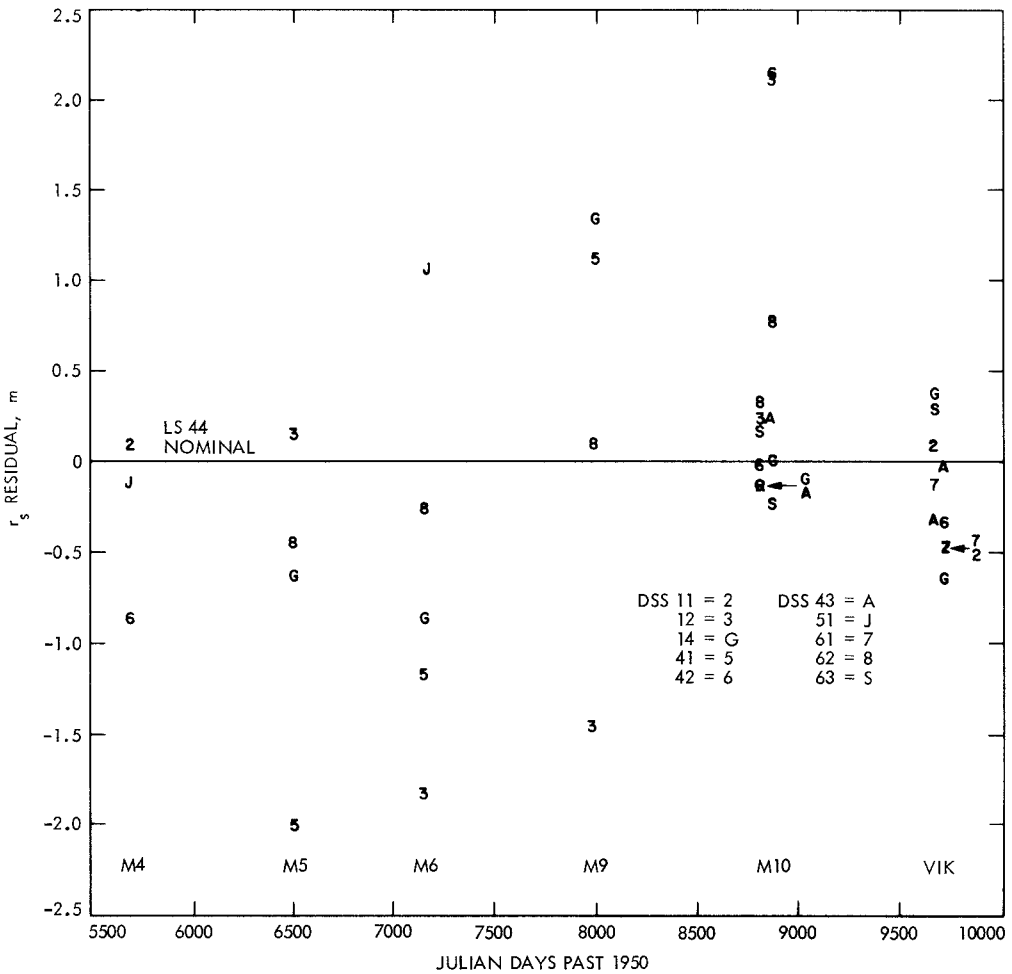

Fig. 14. DE 84 r_s residuals after estimating precession and polar motion

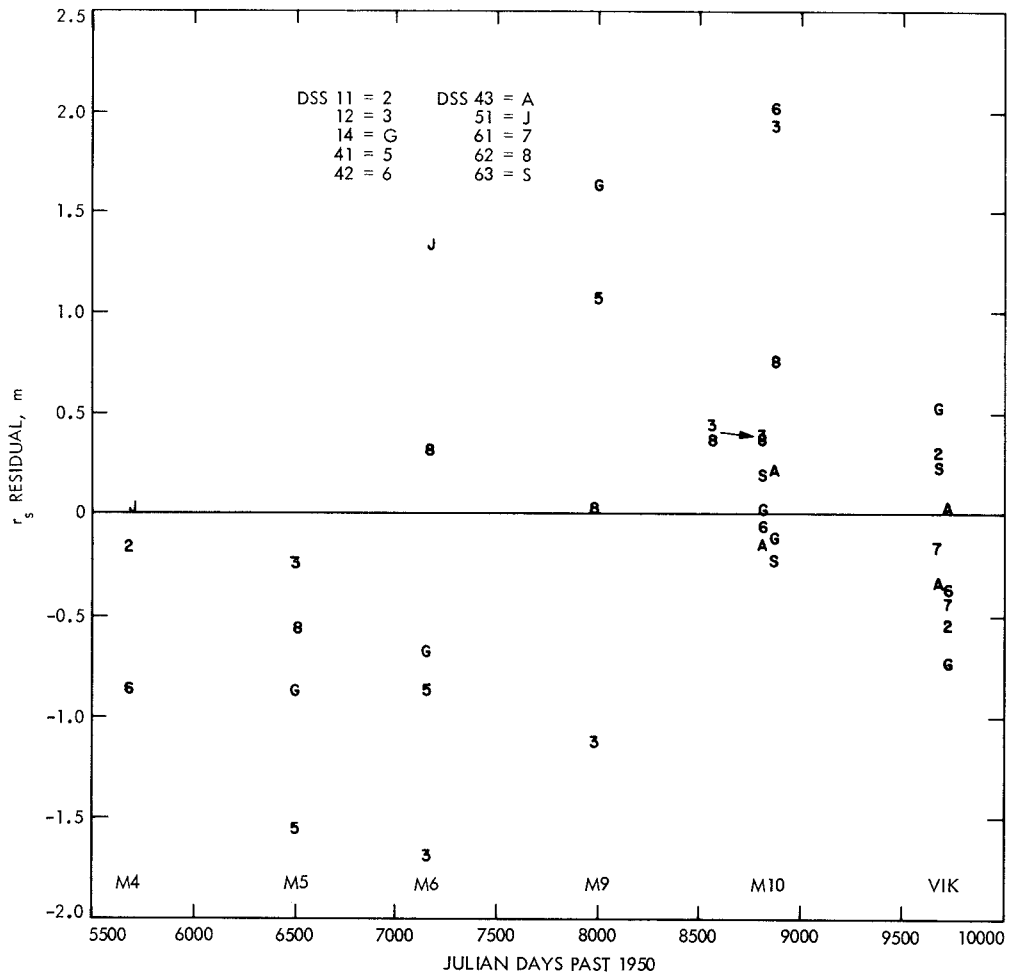

Fig. 15. DE 96 r_s residuals after estimating precession and polar motion